Received: 14 May 2022 | Accepted: 13 August 2022

DOI: 10.1002/bab.2400

ORIGINAL ARTICLE

WILEY

Development of a "turn off–on" whole-cell biosensor for sulforaphane detection based on the ultrasensitive activator HrpRS

Renjie Li[1] | **Shengyan Chen**[1] | **Yangguang Li**[1] | **Xuan Chen**[1] | **Bang-Ce Ye**[1,2,3]

[1]Key Laboratory for Green Processing of Chemical Engineering of Xinjiang Bingtuan, School of Chemistry and Chemical Engineering, Shihezi University, Shihezi 832003, China

[2]Institute of Engineering Biology and Health, Collaborative Innovation Center of Yangtze River Delta Region Green Pharmaceuticals, College of Pharmaceutical Sciences, Zhejiang University of Technology, Hangzhou, Zhejiang, China

[3]Laboratory of Biosystem and Microanalysis, State Key Laboratory of Bioreactor Engineering, East China University of Science and Technology, Shanghai, China

Correspondence
Bang-Ce Ye, School of Chemistry and Chemical Engineering, Shihezi University, Shihezi 832003, China.
Email: bcye@ecust.edu.cn

Abstract

Sulforaphane (SFN), a defense secondary metabolite, can be used to predict the health status of plants and also has pharmacological effects, including anticancer, antioxidant, and anti-inflammatory properties. The detection of SFN is therefore of great significance for the prevention and treatment of diseases. In this study, a "turn off" whole-cell biosensor that can rapidly and robustly respond to the presence of SFN was constructed based on the orthogonal genetic components (*hrpR*, *hrpS*, and P_{hrpL}) of *Pseudomonas syringae* (PS). The final optimized biosensor, p114(30R-30S), was able to inhibit 91.7% of the fluorescence intensity in the presence of 100-μM SFN. Subsequently, a HrpRS-regulated OFF–ON genetic switch was designed by reconstituting a reverse σ^{70} promoter on the σ^{54}-P_{hrpL} promoter sequence; this was coupled with dual-color reporter genes to construct a "turn off–on" whole-cell SFN biosensor. The P_{hrpLB} variant increased the expression of green fluorescence a factor of 11.9 and reduced the expression of red fluorescence by 85.8% compared with the system in the absence of SFN. Thus, a robust switching of signal output from "turn off" to "turn on" was realized. In addition, the biosensor showed good linearity in the SFN concentration ranges of 0.1–10 μM ($R^2 = 0.99429$) and 10–100 μM ($R^2 = 0.99465$) and a detection limit of ~0.1 μM.

KEYWORDS
dual-color sensor, genetic switch, promoter modification, sulforaphane detection, whole-cell biosensor

1 | INTRODUCTION

Gram-negative bacilli activate σ^{54}-dependent transcription at the P_{hrpL} promoter via the enhancer-binding proteins HrpR and HrpS (HrpRS); this triggers the Type III secretion system (TTSS) to inject toxic effector proteins into the cells of the host plant in order to exert a virulent effect or induce a hypersensitive response in nonhost plants.[1–4] The *hrp* gene cluster (*hrpR*, *hrpS*, *hrpV*, *hrpG*, and *hrpL*) sequentially activate the expression of the components of the TTSS in a programmed manner. Based on the properties of the *hrp* gene cluster, synthetic biologists

Abbreviations: LB, Luria–Bertani; PS, *Pseudomonas syringae*; RBS, ribosome binding site; SFN, sulforaphane; TTSS, Type III secretion system.

construct amplifiers, logic gates, and gene regulatory cascades that control and reprogram the signal processing pathways in cells in order to realize advanced intracellular and extracellular control functions.[5–8] However, until now, the ligands that directly regulate the orthogonal components (i.e., *hrpRS*, *hrpV*, and P_{hrpL}) and the sensing genetic circuits associated with these components have not been identified.

Studies have shown that sulforaphane (SFN) can covalently modify cysteine at position 209 of HrpS to inhibit the activity of HrpS.[9] SFN is a defense secondary metabolite with high chemical reactivity and biological activity; it is produced by the hydrolysis of glucosinolates by myrosinases under the loss of cellular integrity or other environmental stimuli.[10,11] This process allows plants to grow healthily despite exposure to natural environments that are overloaded with microorganisms; it is thus considered to be a primary cause of insect resistance in plants.[12,13] SFN is not only associated with insect resistance in plants, but also is linked with anticancer,[14,15] antioxidant,[16,17] anti-inflammatory,[18,19] and antibacterial[20,21] properties; it is also known to improve resistance to neurodegenerative diseases in mammals.[22] As a breakdown product of glucosinolates, tissues contain basal levels of SFN in the absence of cell damage, but SFN concentrations dramatically increase on the occurrence of tissue damage or cell death.[13,23] The change in SFN concentrations thus, indicates the health status of plant cells. Currently, SFN concentrations are determined primarily using analytical techniques that involve complex sample processing procedures, which can lead to inaccurate results.[24,25] Therefore, it is urgent to construct sensing genetic circuits that can respond to SFN with high ease of use, low cost, and high sensitivity, based on the characteristics of *hrpRS* and P_{hrpL}.

Whole-cell biosensors have been rapidly developed in the fields of environment detection, health monitoring, and biosynthesis because they are robust, ecofriendly, and cost effective; these whole-cell biosensors permit the detection of SFN.[26–28] "Turn off" whole-cell biosensors frequently lack sensitivity and have problems related to difficult visualization due to their working mechanism. In order overcome these issues, synthetic biologists have implemented a series of OFF–ON genetic switches, which are based on native switches that switch the output "turn off" to "turn on," so as to reprogram the cell behavior.[29,30] The most characteristic switch is the toggle switch, which consists of any two repressible promoters arranged in a mutually inhibitory network.[31–35] Since this requires additional regulatory systems and ligand induction, it is not feasible to utilize such bistable logic switches for the precise monitoring of small molecules.[36] Another type of genetic switch is based on site-specific recombinases that can cut and rejoin DNA at specific recombination sites; this results in repeated switching between two steady states.[37–39] Due to the heritability and accumulative effect of recombinases on the recombination switching of promoter DNA, recombinase-based logic switches tend to result in a higher background.[40] It is therefore necessary to develop a logic switch directly regulated by transcription factors.

An HrpRS-regulated toggle switch was designed based on the reconstitution of a reverse σ^{70} promoter on the σ^{54}-P_{hrpL} promoter sequence. This was coupled with a dual-color reporter system to construct "turn off–on" biosensors. When the SFN is absent, the HrpRS occupies the space on the −12 and −24 sites of the σ^{54} promoter, which results in the excitation of red fluorescence (mRFP1). When the SFN is present, the SFN binds to the HrpS protein to detach HrpRS complex from the −12 and −24 sites of the σ^{54} promoter, exposing the −10 and −35 sites of the σ^{70} promoter, which can be identified by high-affinity RNA polymerase, resulting in the excitation of green fluorescence (GFP) and the inhibition of the red fluorescence. The switching of the toggle switch is thus achieved by controlling the presence (or absence) of HrpRS. The genetic switch we designed can be modularly applied to other sensing circuits or dynamic regulatory networks in order to promote the development of synthetic biology.

To this end, in this work we developed an SFN-responsive "turn off–on" whole-cell biosensor. First, we constructed a "turn off" SFN biosensor based on the HrpRS/P_{hrpL} regulatory system. With the addition of the inducer SFN, the activity of the red fluorescence was inhibited. The p114(30R-30S) variant was found to have a fluorescence inhibition efficiency of 91.7% upon addition of 100-μM SFN. Next, we induced a series of mutations in the σ^{54}-P_{hrpL} promoter sequence to design an OFF–ON genetic switch. Consequently, we obtained an SFN-inducible "turn off–on" whole-cell biosensor variant P_{hrpLB}, with a 11.9-fold increase in the induction ratio of green fluorescence when 100-μM SFN was added. The limit of detection of the P_{hrpLB} variants was 0.1 μM. This represents the first reported whole-cell biosensor that can be used to detect SFN.

2 | MATERIALS AND METHODS

2.1 | Bacterial strains, growth conditions, and reagents

Plasmid cloning and biosensor characterization were performed in the *Escherichia coli* DH5α and *E. coli* TOP10 strains. Bacteria were cultured in a Luria–Bertani (LB) (tryptone 10 g/L, yeast extract 5 g/L, NaCl 10 g/L) medium

under aerobic conditions; the solid medium was supplemented with 15 g/L agar on the basis of the LB broth. During cloning and incubation, kana antibiotics (50 μg/mL) and ampicillin (100 μg/mL) were used as selectable markers. Pick a single colony from freshly streaked plates and inoculate them into 15 ml universal tubes containing 5 mL of fresh LB broth and inoculate overnight in a shaker (200 rpm) at 37°C. SFN and the other chemicals used (3-butenyl, 4-pentenyl, methyl isothiocyanate; isopropyl isothiocyanate, phenethyl isothiocyanate, benzyl isothiocyanate, 4-pentenenitrile, 3-phenylpropionitrile, goitrin, and indole-3-carbinol) were of analytical grade and were obtained from Sigma–Aldrich.

2.2 | Construction of the sensing and reporting modules for the SFN-responsive biosensors

The plasmids and primers used in this study are described in detail in the Supplementary Information (see Tables S1 and S2). The detailed sequences of genetic parts are presented in Table S3. The plasmids used for the SFN sensing module were all constructed using pSB4A3 as the backbone, whereas the construction of the reporting module was based on pSB3K3. Molecular cloning experiments such as polymerase chain reaction (PCR), DNA purification, homologous recombination, transformation, colony PCR, and plasmid extraction were performed. The target gene *hrpR* (containing the ribosome binding site [RBS] B0030(RBS30)), *hrpS* (containing the RBS30 and the terminator B0015), and the promoter P_{hrpL} sequences are all biosynthesized by Goldwisdom.com. The construction of the sensing module was undertaken using the following procedure. Vector pSB4A3 was linearized using the primer pair Sfix-F and Pfix-R. The genes *hrpR* (containing the RBS30) and *hrpS* (containing the RBS30 and B0015) were amplified from the synthetic plasmid carrying the *hrpRS* gene using the primer pairs R30-hrpR-F and hrpR-R30-R and R30-hrpS-F and hrpS-R, respectively. Using the amplified *hrpR* fragment as a template and J109-FF and hrpR-R30-R as a primer pair, a second amplification was then performed to obtain a J109-RBS30-hrpR fragment containing a constitutive promoter. A third amplification was subsequently performed using J109-RBS30-hrpR as a template and J109-SF and hrpR-R30-R as a primer pair in order to obtain the TYB-J109-RBS30-hrpR fragment containing a homologous arm. Via overlap extension PCR (OE-PCR), the TYB-J109-RBS30-hrpR and hrpS fragments were overlapped and spliced to obtain TJ109-R30-hrpRS, which was then homologously recombined with the linearized pSB4A3 vector to generate a pRL109(30R-30S) plasmid. The construction of other sensing modules followed a similar procedure to that reported above.

For the reporting module, the fragments of *hrpL* and mrfp1 (containing the RBS30 and B0015) were amplified from the synthetic plasmid carrying the promoter hrpL gene and the existing plasmid carrying mrfp1 using the primer pairs hrpL-F and hrpL-R and R30 mRFP1-F and mRFP1B15-R, respectively. Linearization of the backbone pSB3K3 was performed using the primer pair Sfix-F and Pfix-R. The mrfp1 gene was fused downstream of the inducible promoter P_{hrpL} via fusion PCR, and it was then homologously recombined with the linearized pSB3K3 vector to generate a pRLhrpL-mRFP1 plasmid.

2.3 | Modification of sensing modules for response to SFN

To modulate the intracellular receptor density, a response to SFN was engineered in the biosensor. The pathway used is PCR, replacing the constitutive promoter and RBS that directly activate HrpRS expression. The specific method used here was as follows: first, using the primer pairs RC-hrpR-F and hrpR-RC-R, RC-hrpS-F, and hrpS-R were used to amplify the RC-hrpR (containing the RBS) and RC-hrpS (containing the RBS and B0015), respectively, from the synthetic plasmid carrying the *hrpRS* gene. Then, using the RC-hrpR fragment as a template and JC-FF and hrpR-RC-R as a primer pair, a second amplification was performed to obtain a JC-RC-hrpR fragment containing the corresponding constitutive promoter and RBS. Finally, a third amplification was performed using JC-RC-hrpR as a template and JC-SF and hrpR-RC-R as a primer pair to obtain the TYB-JC-RBS-hrpR fragment containing the homologous arm. By OE-PCR, the TYB-JC-RBS-hrpR and RC-hrpS fragments were overlapped and spliced to obtain TJc-RC-hrpR-RC-hrpS, which was then homologously recombined with the linearized pSB4A3 vector to generate the pRLC(CR-CS) plasmid. The construction of other engineered biosensors followed a similar procedure to that described above.

2.4 | Construction of logical toggle biological switches

The *gfp* gene (containing the RBS30 and B0015) was amplified from the existing plasmid that carries the *gfp* gene using the primer pair R30GFP-F and GFPB15-R. Following a PCR product purification, it was homologously recombined with linearized pRLhrpL-mRFP1 (obtained using the pFix-F and sFix-R primer pair) to generate 30GFP-PhrpLWT-30 mRFP1, referred to here as PhrpLWT. The

mRFP1 gene is under the control of the P_{hrpL} promoter, and the −10 and −35 sites of the σ^{70} promoter are formed via site-directed mutation of the promoter; this is in the opposite direction to that controlling the mRFP1 gene expression. Linearized 30GFP-t-PhrpLWT-30 mRFP1 (containing the mutation sites) was amplified using PhrpLWT as a template and PhrpLA-F and PhrpLA-R as a primer pair. Subsequently, the digestive enzyme Dpn I was added in a 37°C water bath for 30 min and the transformation was carried out. All variants were generated via similar methods and all biosensors took the same name as their respective promoters.

2.5 | Fluorescence measurements and data analysis

Single colonies of the *E. coli* TOP10 strain containing the validated double plasmid were incubated overnight at 37°C in 2 mL of LB supplemented with 50 μg/mL of kanamycin and 100 μg/mL of ampicillin in 24-well deep-well plates (Canvic, China). The absorbance at 600 nm, OD_{600}, was then measured using a microplate reader (BioTek Instruments, Winooski, VT, USA), and the overnight cultures were subsequently diluted to $OD_{600} \approx 0.02$ in the LB medium supplemented with 50 μg/mL of kanamycin and 100 μg/mL of ampicillin. One hundred ninety-eight microliters of the diluted overnight culture was transferred to black 96-well plates (Fluotrac 200; Greiner, Germany). Two microliters of SFN of different concentrations (all samples in triplicate) was added to the above dilution culture. The plates were incubated in the microplate thermostat shaker (MB100-4A, China) at 37°C and 1000 rpm for 6 h. The OD_{600} and fluorescence (excitation at 584 nm and emission at 620 nm or excitation at 485 nm and emission at 520 nm, sensitivity = 100%) were read using the microplate reader. The signal output of the different biosensors for a range of SFN concentrations was evaluated considering Fluo/OD_{600} (Fluorescence/OD_{600}).

The time-dependent specificity response experiments of the biosensors and the fluorescence changes of the switches were also performed on black 96-well plates. To measure the changes in the fluorescence of the cell cultures, 2 mL of the culture samples was collected after 6 h of incubation with the addition of the inducer. Cells were harvested via centrifugation at 12,000×*g* for 1 min, washed 3 times with 1 mL of phosphate-buffered saline solution (pH 7.4) and finally cell pellets were harvested via centrifugation at 12,000×*g* for 1 min.

The background fluorescence was determined using blank wells that contained only the LB medium; this reading was subtracted from the readings obtained from the other wells. The fluorescence inhibition efficiency of the SFN-responsive biosensor was calculated according to:

$$\text{Fluorescence inhibition efficiency} = \frac{\text{RFU (SFN)} - \text{RFU (control)}}{\text{RFU (control)}} \times 100\%$$

where RFU (SFN) and RFU (control) denote the average reading of Fluo/OD_{600} from the triplicates in wells containing the bacteria biosensor in the presence or absence of SFN, respectively. The fold-change in relative fluorescence was calculated according to:

$$\text{fold-change in relative fluorescence} = \frac{\text{Fluo/OD}_{600}\ (+\text{inducer})}{\text{Fluo/OD}_{600}\ (-\text{inducer})}$$

where Fluo/OD_{600} (+ inducer) and Fluo/OD_{600} (− inducer) represent the fluorescence in the presence and absence of the inducer, respectively, after the specified incubation period.

2.6 | Real sample analysis

Fresh broccoli (Cruciferous, Brassica) was purchased from a local market and chopped with a knife. 2.0 g (accurate to 0.0001 g) of chopped broccoli was weighed into a 50 mL centrifuge tube and 10.0 mL of pH = 3.0 hydrochloric acid aqueous solution was added and mixed well, and then it was placed in a 35°C water bath for 30 min. After cooling to room temperature, 20 mL of ethyl acetate was added and vortexed for 1 min, then centrifuged at 5000×*g* for 5 min at 4°C. The organic layer was concentrated to dryness in a rotary evaporator at 45°C. Dissolved with 1 ml of dimethy sulfoxide and filtered through a 0.45 μm membrane filter, then diluted 25-fold for high performance liquid chromatography (Waters, USA) analysis. Chromatographic conditions: Column: C_{18} column (5 μm, 250 mm × 4.6 mm; Waters); Column temperature: 35°C; mobile phase: acetonitrile/water (20/80, v/v); flow rate: 0.8 ml/min; detection wavelength: 245 nm; injection volume: 2 μL.

Samples were diluted to the appropriate concentration with dimethyl sulfoxide. Various concentrations (0, 5, 10, 20, 40, and 80 μM, all samples in triplicate) of SFN were added to the samples. The bacteria were grown overnight in LB medium supplemented with 50 μg/mL of kanamycin and 100 μg/mL of ampicillin, and the overnight cultures were then diluted with LB medium (50 μg/mL of kanamycin and 100 μg/mL of ampicillin) to $OD_{600} \approx 0.02$. The inducers were added to 200 μL aliquots of bacterial culture in 96-well plates and incubated at 37°C for 6 h. The SFN concentration in the samples was then estimated on the basis of the standard curve equation.

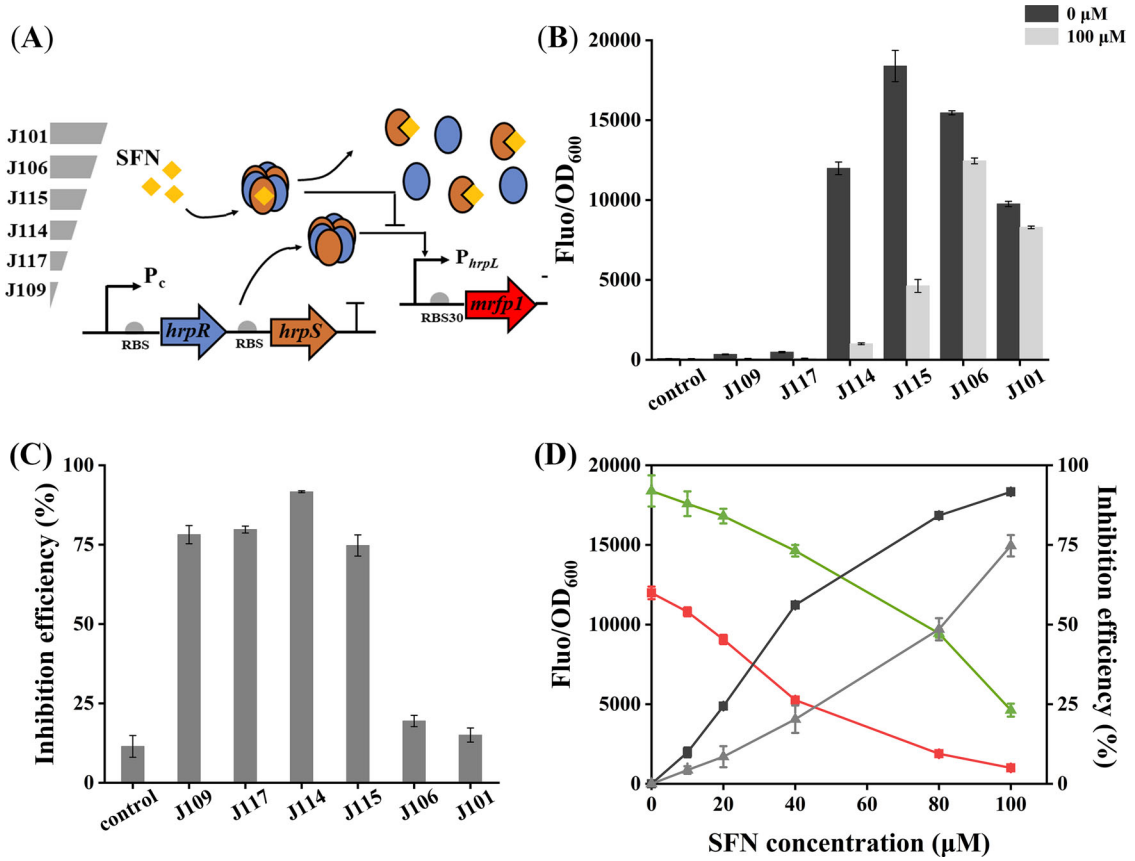

FIGURE 1 Feasibility analysis of the whole-cell biosensors based on the response of HrpRS to SFN. (A) The construction of a genetic circuit for SFN-responsive biosensors. The strength of constitutive promoters decreases sequentially from top to bottom. (B) The fluorescence of biosensors containing different activity promoters (controls: pSB3K3 and pSB4A3 vector backbones). (C) The fluorescence inhibition efficiency of biosensors in response to 100-μM SFN. (D) The fluorescence output and fluorescence inhibition efficiency of the p114(30R-30S) and p115(30R-30S) biosensors in response to SFN (in concentrations from 0 to 100 μM). The green and gray triangles represent the fluorescence output and fluorescence inhibition efficiency of J115, respectively, and the red and black squares represent the fluorescence output and fluorescence inhibition efficiency of J114. Error bars represent the standard deviation from the arithmetic mean ($n = 3$).

3 | RESULTS AND DISCUSSION

3.1 | Construction of biosensors with a red fluorescence readout

The detection of SFN provides a reference for the prevention of diseases and insect-related problems in plants. In order to efficiently detect SFN, we developed a "turn off" SFN whole-cell biosensor based on the properties of *hrpRS* and *hrpL* (Figure 1A). The engineered biosensor consists of two parts: a sensing module and a reporting module. The sensing module expresses the proteins HrpR and HrpS, which combined to form a heterohexameric complex to function. The complex can then bind to an inducible promoter, P_{hrpL}, which activates the expression of the reporting module. For use as a reporting module, we designed a system based on a red fluorescent protein where the HrpRS complex activates the expression of mRFP1. The key transcription factor, HrpRS, was driven under the control of a constitutive promoter. In the presence of the inducer SFN, HrpRS dissociates from its cognate promoter, P_{hrpL}, and the reporter gene was thus inhibited. The same result can also be achieved via the HrpV protein; an inhibitor of P_{hrpL} directly interacts with HrpS to inhibit the activity of HrpRS. However, because the expression of HrpV needs to be induced by other regulatory systems, this increases the bacterial growth burden and also delays the regulatory effect.[7,41]

Six SFN-responsive whole-cell biosensors with *hrpRS* sensing modules driven by six constitutive promoters of varying transcriptional strengths were constructed and examined for fluorescence changes in the presence of 100-μM SFN. It was found that the signal output first increased and then decreased with increasing promoter activity, regardless of the presence or absence of SFN (Figure 1B). The J115 (p115(30R-30S)) had the highest

signal output (18389) among the six biosensors in the absence of SFN, while the J114 (p114(30R-30S)) exhibited the highest inhibition efficiency (91.7%) when exposed to 100-μM SFN (Figures 1B and C). The biosensor driven by the high activity promoter J101 performed poorly both in the fluorescence output and inhibition efficiency; this may be due to the high concentration of SFN and the strong activity promoter exacerbating the cellular burden (Figure S1). The performance of the strains p114(30R-30S) and p115(30R-30S) was subsequently examined under a range of SFN concentrations. As shown in Figure 1D, the fluorescence output of p114(30R-30S) at each concentration was lower than that of p115(30R-30S), but the inhibition efficiency was significantly better in the case of p114(30R-30S) relative to that of p115(30R-30S). We hypothesize that the expression of HrpRS driven by the weaker promoter J114 was small, so the signal output was lower, and the fluorescence was thus more easily inhibited. Bacterial growth was significantly inhibited in the presence of high concentrations of SFN (Figure S1); SFN at concentrations higher than 100 μM could not be used due to the toxic effects of the SFN on cell growth and viability. The above results indicate that the coupling of the *hrpRS* sensing module and the mRFP1 reporting module successfully detects SFN, and the expression level of the HrpRS was closely related to the performance of the biosensors.

3.2 | Effects of the translation level of HrpRS on the SFN biosensors

The transcription factor HrpS effectively inhibits the expression of fluorescence of the proteins by binding to the SFN, and the fluorescence inhibition efficiency improved with increasing SFN concentrations. However, high concentrations of SFN burdened the bacterial growth. Controlling the expression level of HrpRS by balancing the promoter activity and the strength of the RBS in the sensing module represents an effective strategy to further increase the fluorescence output and fluorescence inhibition efficiency without damaging the bacteria.

To obtain a stronger signal output and higher fluorescence inhibition efficiency, we constructed a series of variants with the RBS sequences of different translation strengths in front of the *hrpR* and *hrpS* genes.[5] First, we replaced the RBS30 (B0030) with the weaker RBS (B0031, B0032, and B0033) to construct p115(CR-CS) variants. It can be seen that under the same promoter and the same concentration of SFN, the fluorescence decreased with reduced expression of HrpR and the performance of the p115(30R-32S) biosensor was significantly better relative to the other variants (Figure 2A). The biosensors performed better when the expression of *hrpS* was lower than that of *hrpR*. This further indicates that the expression level of the HrpS was related to the performance of the biosensors. The fluorescence output and fluorescence inhibition efficiency of the engineered biosensors p115(30R-32S) and p114(30R-30S) induced by a range of SFN concentrations were then analyzed. The fluorescence of p114(30R-30S) was stronger than that of p115(30R-32S), but the fluorescence inhibition efficiency was smaller in the case of p114(30R-30S) compared with that of p115(30R-32S). The fluorescence inhibition efficiency of p115(30R-32S) was three times greater than that of p114(30R-30S) when induced by 10-μM SFN; the inhibition efficiency reached approximately 80% with the addition of 40-μM SFN (Figure 2B). When different strengths of the RBS were coupled with strong promoters (such as J106 or J101), we found that the expression level of HrpR largely determined the fluorescence intensity of the biosensor, whereas the HrpS expression level determined the fluorescence inhibition efficiency (Figures S1S2 and S3). The fluorescence intensity was negatively correlated with the fluorescence inhibition efficiency. Systematic tests were performed on the promoters and RBS and compared with previous reports; we inferred that a single strategy of engineering modification, such as the enhancing promoter activity or improving the RBS strength, was not sufficient to obtain sufficient sensing performance; thus we consider the relationship between promoter activity and RBS strength.

3.3 | Dose-dependent response to SFN

To examine the dose-dependent responses of the best-performing variants (p114(30R-30S) and p115(30R-32S)) to SFN, the two biosensors were stimulated at a range of SFN concentrations (0, 0.1, 0.3125, 0.625, 1.25, 2.5, 5, 10, 20, 40, 80, and 100 μM). The results were shown in Figure 3. The p114(30R-30S) variants showed a larger signal output range than the p115(30R-32S) variants, but the p115(30R-32S) exhibited a higher fluorescence inhibition efficiency in response to low concentrations of SFN; the inhibition efficiency of p115(30R-32S) was 10.6% in the presence of 0.1-μM SFN (Figures 3A and B). A good dose-dependent induction response of the biosensors for SFN occurred at two different ranges of concentration. A linear relationship between the inhibition efficiency of the p114(30R-30S) variant and the concentration was found in the range of 0.1–12.47 μM ($R^2 = 0.99619$) and 12.47–100 μM ($R^2 = 0.99235$) (Figure 3C), and the p115(30R-32S) variant was found to show a linear relationship between the inhibition efficiency and concentration in the concentration ranges 0.1–7.38 μM ($R^2 = 0.99449$) and 7.38–100 μM ($R^2 = 0.90412$) (Figure 3D).

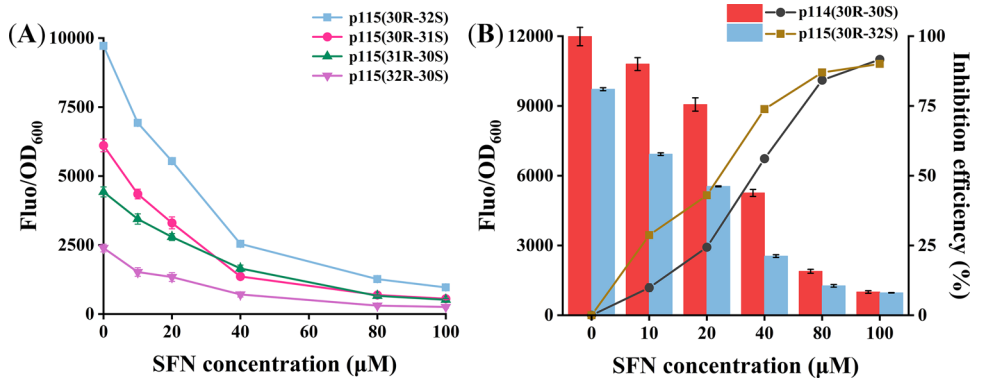

FIGURE 2 Performance characterization of the engineered biosensors in response to SFN. (A) The fluorescence output of the biosensors in response to the SFN concentrations when J115 couples a range of RBS strengths to drive the expression of HrpRS. (B) The fluorescence output and fluorescence inhibition efficiency of the p114(30R-30S) and p115(30R-32S) biosensors. The errors shown in the figures were obtained from three experiments ($n = 3$).

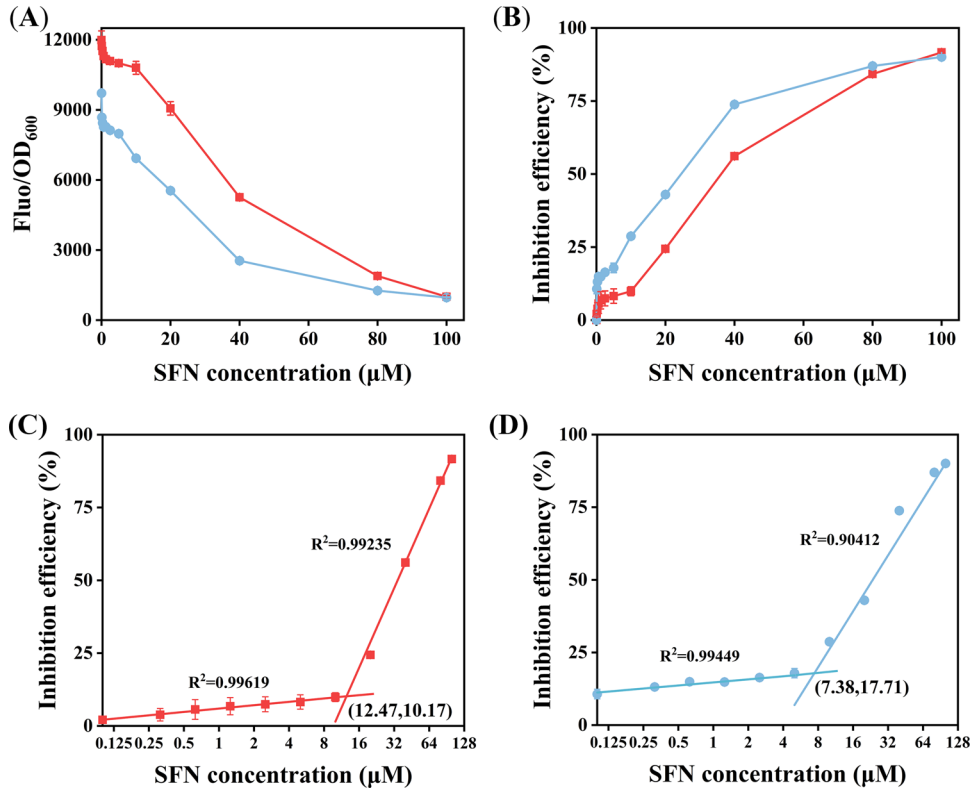

FIGURE 3 Dose-dependent responses to SFN. (A) Dose–response curves of the biosensors p114(30R-30S), red squares, and p115(30R-32S), blue circles, when exposed to SFN concentrations ranging from 0 to 100 μM. (B) The fluorescence inhibition efficiency of the biosensors when exposed to SFN with concentrations ranging from 0 to 100 μM. (C) The linear fit parameters for the p114(30R-30S) biosensor for SFN concentrations from 0.1 to 100 μM. (D) The linear fitting parameters for the p115(30R-32S) biosensor for SFN concentrations from 0.1 to 100 μM range. (C and D) Data from (B). The errors shown in the figures were obtained from three experiments ($n = 3$).

3.4 | Dynamics and specificity of the SFN-responsive biosensor

For biosensors that are stimulated by SFN, the response time and specificity are important factors that should be considered for possible applications. The bacterial cultures were exposed to 100-μM SFN for different incubation periods (from 0 to 12 h). Figures 4A and B show the time-dependent analysis of the biosensors p114(30R-30S) and p115(30R-32S). The fluorescence inhibition efficiency

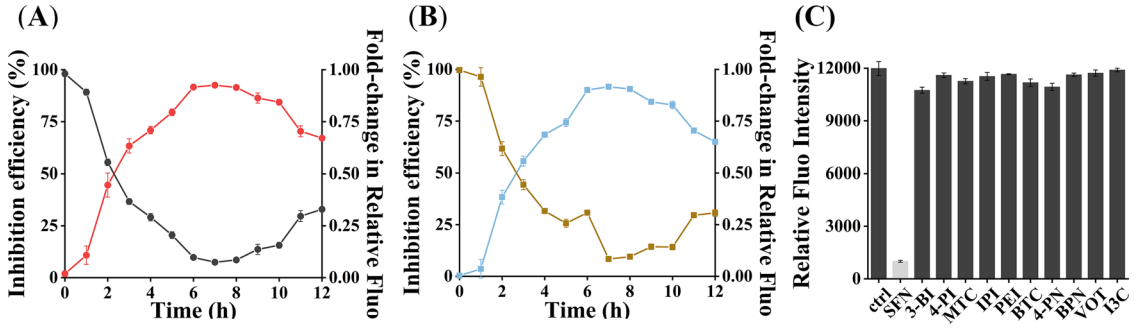

FIGURE 4 Response dynamics and specificity of SFN-induced bacterial biosensors. (A) The inhibition efficiency and fold-change in the relative fluorescence of the p114(30R-30S) biosensor in response to 100-μM SFN over the time period 0–12 h. (B) The inhibition efficiency and fold-change in the relative fluorescence of the p115(30R-32S) biosensor in response to 100-μM SFN over the time range 0–12 h. (C) The selectivity of the p114(30R-30S) biosensor detection of SFN and other kinds of secondary metabolites (the concentration of all metabolites considered was 100 μM). The errors bars shown in the figures were obtained from three experiments ($n = 3$)

of p114(30R-30S) was higher than that of p115(30R-32S) within 6 h, and the fluorescence inhibition efficiency of the p114(30R-30S) reached approximately 11% in 1 h, far exceeding the inhibition efficiency of p115(30R-32S) (3.6%). The inhibition efficiency of the two variants was found to reach approximately 70% within 4 h. Meanwhile, the fold-change in the relative fluorescence of p114(30R-30S) was steeper than that of p115(30R-32S) over 6 h. This result indicates that the response of p114(30R-30S) to SFN is faster than that of p115(30R-32S). The response of the biosensors reached their maximal values at around 6 h; this maximum was followed by a gradual decreased in inhibition efficiency after 7 h. We thus, infer that the partial decomposition of SFN may occur and the HrpS bound to it was thus released, which in turn coupled with the HrpR to activate the expression of mRFP1. It was observed that the greater the concentration of SFN to which the bacterial cultures were exposed, the greater the fold-change in the relative fluorescence (Figure S4). Due to the instability of SFN, the time-dependent experiments were only carried out for durations up to 12 h and were not exposed to light during the experiments. As shown in Figure 4C, p114(30R-30S) exhibits a specific response to SFN without obvious fluorescence inhibition due to other kinds of secondary metabolites. This result indicate that the developed biosensor has an excellent selectivity to SFN.

3.5 | Design and characterization of logic toggle biological switches

The conserved regions of the σ^{54}-dependent promoter *hrpL* are distributed at the −12 and −24 sites upstream of the transcription start site. To design a genetic switch that robustly switches the signal output from "turn off" to "turn on", we reversely formed the −10 (TATAAT or GATACT) and −35 (TTTACA or TTGACA) sites of a constitutive promoter regulated by the housekeeping factor σ^{70} via site-directed mutation on the σ^{54}-P_{hrpL} and coupled this with a dual-color reporter gene to construct a "turn off–on" SFN whole-cell biosensor that can realize the conversion of the fluorescence color from red to green (Figure 5A). The expression of the HrpRS can be regulated either by a constitutive promoter or coupled with other gene circuits capable of acting as a sensor, enabling the detection of a variety of small molecules (Figure 5B).

As shown in Figure 5C, we constructed a series of variants under the principle of introducing minimal mutations in the genetic sequence. These variants and the wild-type promoter were analyzed under 100-μM SFN induction. Our results showed that the mutated variants exhibited a significant increase in their green fluorescence output compared with the wild-type when exposed to 100-μM SFN, whereas the red fluorescence output of the mutated variants was lower than that of the wild-type in the absence of SFN (Figure 6A). This suggests the feasibility of designing logic toggle switches via site-directed mutation of the promoter. Comparing variants with different mutations at the same position (P_{hrpLA} and P_{hrpLB}, P_{hrpLC} and P_{hrpLD}, and P_{hrpLF} and P_{hrpLG}), we see that the stronger the constitutive promoter activity, the lower the green fluorescence intensity (Figure 6A). The variant P_{hrpLD} showed the highest green fluorescence output compared with the other variants, but it showed a low level of induced fold-change due to high background fluorescence (Figures 6A and S5a). The P_{hrpLB} variant with its medium inducible activity showed a 11.9-fold induced change, and its red fluorescence output and inhibition efficiency were lower than the wild-type only (Figures 6A and S5b). This result indicated that the binding of the transcription factor HrpRS to the σ^{54} promoter and the binding of the RNA polymerase to the σ^{70}

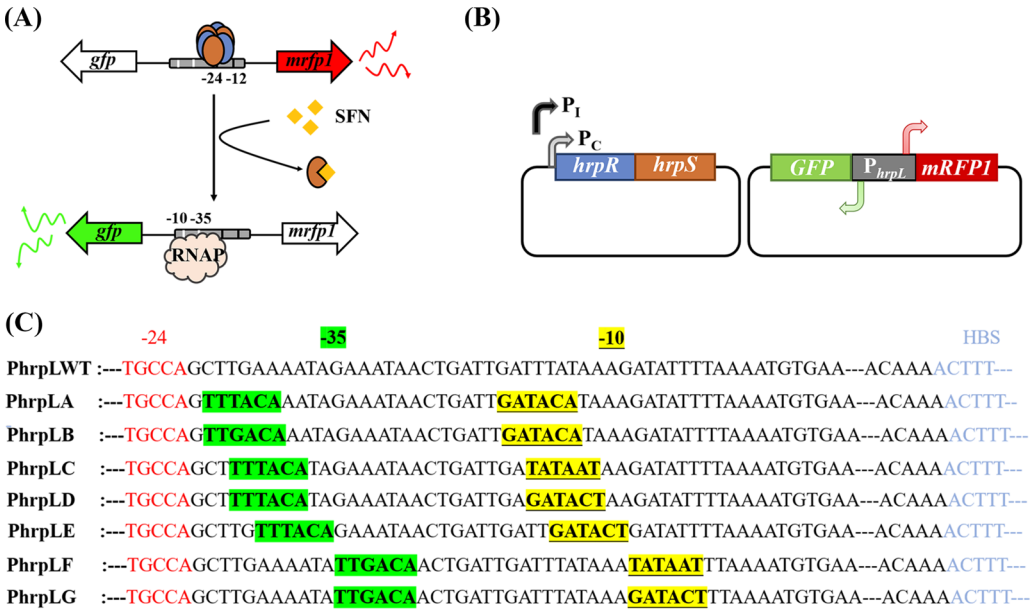

FIGURE 5 Design of logic toggle biological switches. (A) A schematic depicting the operation of the logic toggle switches. The constitutive promoter (J114) is placed upstream of the HrpRS recombinase-encoding sequence in one plasmid. The second plasmid encodes a fluorescent reporter switch composed of two fluorescent protein genes (*mRFP1* and *GFP*) and an inducible promoter (P_{hrpL}) containing a constitutively active promoter. (B) Activation of the HrpRS recombinase-encoding sequence can be either induced by constitutive promoters (J109, J117, J114, J115, J106, or J101) or other responsive systems. (C) Construction of the logic toggle switches by site-directed mutagenesis in the wild-type promoter (P_{hrpL}) to form the −10 (underlined and shaded in yellow) and −35 sites (shaded in green) of the constitutive promoters

promoter should be in equilibrium in order to ensure good fluorescence changes.

We selected the P_{hrpLB} variant for further study. To investigate the thresholds of the detection, we examined the fluorescence signal output in terms of analyte concentration. As depicted in Figures 6B and C, the changes in the fluorescence of either GFP or mRFP1 in response to different concentrations of SFN represent good dose–response curves. The increase in the fluorescence intensity of GFP and the decrease in the fluorescence intensity of mRFP1 were detected at SFN concentrations as low as 0.1 μM. Figure 6D shows the switch from red to green fluorescence as a function of increasing SFN concentration.

3.6 | Performance characterization of the "turn off–on" SFN whole-cell biosensor

To test the linearity and the response time of the variant P_{hrpLB} to SFN, the cell cultures were induced at a range of SFN concentrations (from 0 to 100 μM) and were exposed to 100-μM SFN for different incubation periods (from 0 to 12 h). The P_{hrpLB} variant exhibited linear relationships in the concentration ranges of 0.1–10 μM ($R^2 = 0.99429$) and 10 to 100 μM ($R^2 = 0.99465$) (Figure 7A). For an SFN concentration of 100 μM, the P_{hrpLB} biosensor showed a more than twofold increase in green fluorescence within 2 h, while its red fluorescence showed a significant inhibition at 2 h (Figure 7B). This indicates that the P_{hrpLB} biosensor has a very fast response. The performance of the proposed biosensor was compared with that of other reported SFN detection methods, and the results were presented in Table 1.

There are ways to further improve the performance of the biosensors considered here to achieve faster switching of fluorescence signals. Enhancing the degradation rate of mRFP1 is an effective strategy to improve the fluorescence inhibition efficiency. This can be achieved by adding fluorescence quenchers or adding a protein degradation tag to the mRFP1 coding sequence. We therefore hypothesize that logic toggle biological switches created by engineering a promoter to realize a dual-color fluorescence conversion or even coupling with other response systems will become a powerful methodology to realize the detection of multiple small molecules.

3.7 | Real sample analysis

For the analysis of SFN in broccoli samples with P_{hrpLB}, fresh broccoli purchased from local market was used as the samples and extracted SFN from it. The SFN content in

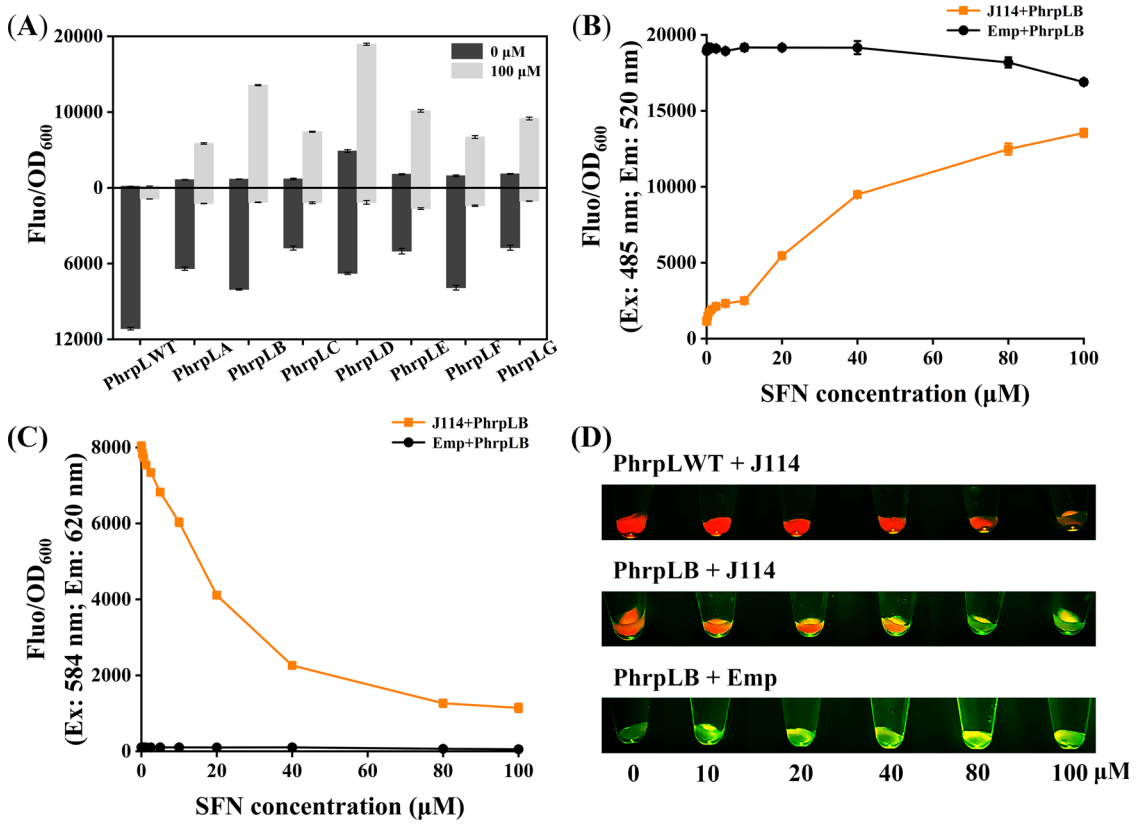

FIGURE 6 Fluorescence changes and dose–response studies of the genetic switches that respond to SFN. (A) Emission at 520 nm (emission of GFP, top) or emission at 620 nm (emission of mRFP1, bottom) were monitored in cell cultures of TOP 10 *E. coli* cells harboring genetic switches in the presence of SFN (the concentration of SFN was 100 μM). Emission at (B) 520 nm and (C) 620 nm of the cell cultures of TOP 10 *E. coli* cells harboring P_{hrpLB} with SFN concentrations ranging from 0 to 100 μM. Emp: pSB4A3. (D) Fluorescence changes in response to varying concentrations of SFN, images of cell pellets were taken using an iPhone and a TGreen transilluminator (TIANGEN BIOTECH). Error bars represent the standard deviation from the arithmetic mean ($n = 3$)

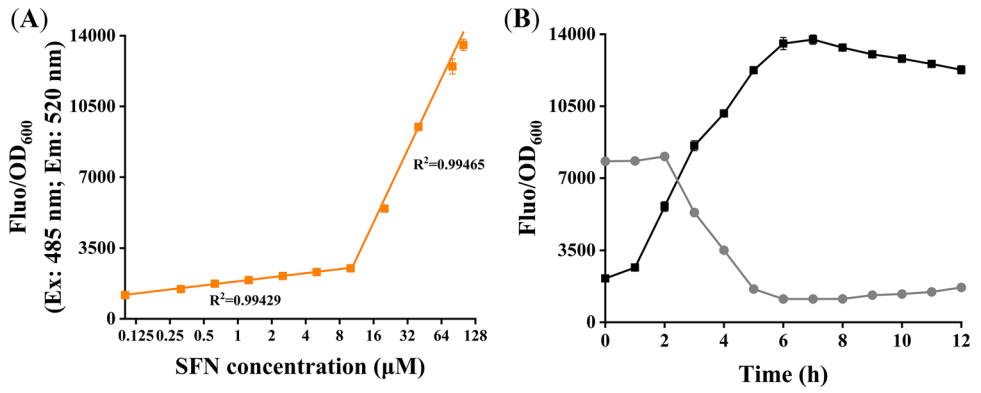

FIGURE 7 Performance characterization of our proposed "Turn off–on" whole-cell biosensor in response to SFN. (A) The linear fit for the P_{hrpLB} biosensor for SFN concentrations from 0.1 to 100 μM. (B) The fluorescence intensity of the P_{hrpLB} biosensor in response to 100-μM SFN over 0–12 h (black squares: GFP and gray circles: mRFP1). The error bars represent the standard deviation from the arithmetic mean ($n = 3$)

the original broccoli extract was found to be 1.002 mg/g via HPLC (Figure S6 and Table S1). The SFN concentrations of the broccoli samples were calculated using the expression: $Y = 202\log_2(x) + 1857$ (in the range 0.1–10.332 μM) and $Y = 3552\log_2(x) - 9430$ (in the range 10.332–100 μM) (Figure 7A). As shown in Table 2, the recovery of the SFN measured by the P_{hrpLB} biosensor was in the range of 97.8–102.3%, showing good agreement with the actual SFN

TABLE 1 Comparison of the constructed biosensor with other SFN determination methods

Method	Linear range	Detection limit	Recovery	Visualization	References
HPLC	2.5–100 μg/ml	0.4419 μg/ml	98.15–100.39%	N	42
LC–MS/MS	8–1000 μg/kg 10–1250 g/kg	3 μg/kg	–	N	25
UPLC–MS/MS	30–2000 ng/ml	–	101.3–105.6%	N	43
GC	–	–	–	N	44
GC-MS	–	–	–	N	45
gNPs-Pdop-Gr/GCE	0.05–50 μM	10 nM	78.76–97.89% 101.76–106.12%	N	46
HrpRS/P_{hrpL}-mRFP1/GFP	0.1–100 μM	0.1 μM	97.8–102.3%	Red turn Green	This work

TABLE 2 Accuracy and reliability of the constructed biosensor for practical samples

Sample	HPLC (μM)	Add SFN (μM)	Fluo/OD600[a]	Estimated (μM)	Recovery
Broccoli extract	1.131	0	1886 ± 37	1.108	–
	1.131	5	2379 ± 59	5.996	97.8%
	1.131	10	2912 ± 84	11.112	99.8%
	1.131	20	6215 ± 126	21.185	100.3%
	1.131	40	9575 ± 72	40.814	99.2%
	1.131	80	13,213 ± 341	82.998	102.3%

[a]Mean Fluo/OD_{600} (Ex: 584 nm; Em: 620 nm) value ± standard deviation ($n = 3$).

concentration present in the samples. These results indicated that the biosensor exhibited strong anti-interference and good stability in determining the SFN concentration in broccoli. Thus, the constructed biosensor shows potential for use in the practical determination of SFN concentrations in diverse cruciferous plants.

4 | CONCLUSION

In summary, in this work we have developed a "turn off" whole-cell SFN biosensor based on the HrpRS and its cognate promoter σ^{54}-P_{hrpL}. When induced with 100-μM SFN, the fluorescence inhibition efficiency can reach 91.7%. The fluorescence inhibition efficiency was further improved when exposed to lower SFN concentrations via control of the constitutive promoter and the RBS. The detection limit of this biosensor was cat. 0.1 μM. Subsequently, an SFN-responsive "turn off–on" whole-cell biosensor was constructed by designing an OFF–ON-type switch. Upon the addition of SFN, the fluorescence color was switched from red to green, realizing a 11.9-fold increase in the fluorescence intensity of GFP and fluorescence inhibition efficiency of 84.1% for mRFP1 compared with the system without the analyte. By controlling the presence or absence of HrpRS, it is possible to achieve robust switching between bistable states; thus, this logic toggle switch has the potential to be applied in a modular manner to gene regulatory networks to control signal output.

FUNDING

This work was supported by the National Natural Science Foundation of China (Grants 22134003 awarded to B. C. Y.).

CONFLICT OF INTEREST

The authors declare no competing financial interests.

ORCID

Bang-Ce Ye https://orcid.org/0000-0002-5555-5359

REFERENCES

1. Cascales E. Inside the chamber of secrets of the type III secretion system. Cell. 2017;168:949–51.
2. Jovanovic M, Lawton E, Schumacher J, Buck M. Interplay among pseudomonas syringae HrpR, HrpS and HrpV proteins for regulation of the type III secretion system. FEMS Microbiol Lett. 2014;356:201–11.
3. Sanchez-Garrido J, Ruano-Gallego D, Choudhary JS, Frankel G. The type III secretion system effector network hypothesis. Trends Microbiol, 2021. https://doi.org/10.1016/j.tim.2021.10.007
4. Feng F, Zhou J-M. Plant–bacterial pathogen interactions mediated by type III effectors. Curr Opin Plant Biol. 2012;15:469–76.
5. Wang B, Kitney RI, Joly N, Buck M Engineering modular and orthogonal genetic logic gates for robust digital-like synthetic biology. Nat Commun. 2011. 2:1–9.
6. Wang B, Barahona M, Buck M. Engineering modular and tunable genetic amplifiers for scaling transcriptional signals in cascaded gene networks. Nucleic Acids Res. 2014;42:9484–92.
7. Shopera T, Henson WR, Moon TS. Dynamics of sequestration-based gene regulatory cascades. Nucleic Acids Res. 2017;45:7515–26.

8. Wan X, Volpetti F, Petrova E, French C, Maerkl SJ, Wang B. Cascaded amplifying circuits enable ultrasensitive cellular sensors for toxic metals. Nat Chem Biol. 2019;15:540–8.
9. Wang W, Yang J, Zhang J, Liu Y-X, Tian C, Qu B, et al. An arabidopsis secondary metabolite directly targets expression of the bacterial type III secretion system to inhibit bacterial virulence. Cell Host & Microbe. 2020;27:601–13.
10. Román J, Castillo A, Cottet L, Mahn A. Kinetic and structural study of broccoli myrosinase and its interaction with different glucosinolates. Food Chem. 2018;254:87–94.
11. Sugiyama R, Hirai MY Atypical myrosinase as a mediator of glucosinolate functions in plants. Front Plant Sci. 2019. 1008.
12. Piasecka A, Jedrzejczak-Rey N, Bednarek P. Secondary metabolites in plant innate immunity: Conserved function of divergent chemicals. New Phytol. 2015;206:948–64.
13. Andersson MX, Nilsson AK, Johansson ON, Boztaş G, Adolfsson LE, Pinosa F, et al. Involvement of the electrophilic isothiocyanate sulforaphane in arabidopsis local defense responses. Plant Physiol. 2015;167:251–61.
14. Clarke JD, Dashwood RH, Ho E. Multi-targeted prevention of cancer by sulforaphane. Cancer Lett. 2008;269:291–304.
15. Russo M, Spagnuolo C, Russo GL, Skalicka-Woźniak K, Daglia M, Sobarzo-Sánchez E, et al. Nrf2 targeting by sulforaphane: A potential therapy for cancer treatment. Crit Rev Food Sci Nutr. 2018;58:1391–405.
16. Cedrowski J, Dąbrowa K, Przybylski P, Krogul-Sobczak A, Litwinienko G. Antioxidant activity of two edible isothiocyanates: Sulforaphane and erucin is due to their thermal decomposition to sulfenic acids and methylsulfinyl radicals. Food Chem. 2021;353:129213.
17. Bauman BM, Jeong C, Savage M, Briker AL, Janigian NG, Nguyen LL, et al. Dr. Jekyll and mr. Hyde: Oxidizable phenol-generated reactive oxygen species enhance sulforaphane's antioxidant response element activation, even as they suppress nrf2 protein accumulation. Free Radical Biol Med. 2018;124:532–40.
18. Moustafa PE, Abdelkader NF, El Awdan SA, El-Shabrawy OA, Zaki HF. Extracellular matrix remodeling and modulation of inflammation and oxidative stress by sulforaphane in experimental diabetic peripheral neuropathy. Inflammation. 2018;41:1460–76.
19. Liang W, Greven J, Fragoulis A, Horst K, Bläsius F, Wruck C, et al. Sulforaphane-Dependent up-regulation of NRF2 activity alleviates both systemic inflammatory response and lung injury after hemorrhagic shock/resuscitation in mice. Shock: Injury, Inflammation, and Sepsis: Laboratory and Clinical Approaches. 2022;57:221–9.
20. Bonay M, Roux AL, Floquet J, Retory Y, Herrmann JL, Lofaso F,, et al. Caspase-independent apoptosis in infected macrophages triggered by sulforaphane via Nrf2/p38 signaling pathways. Cell death discovery. 2015;1:1–10.
21. Schwab M, Reynders V, Loitsch S, Steinhilber D, Schröder O, Stein J. The dietary histone deacetylase inhibitor sulforaphane induces human β-defensin-2 in intestinal epithelial cells. Immunology. 2008;125:241–51.
22. Schepici G, Bramanti P, Mazzon E. Efficacy of sulforaphane in neurodegenerative diseases. Int J Mol Sci. 2020;21:8637.
23. Esfandiari A, Saei A, McKenzie MJ, Matich AJ, Babalar M, Hunter DA. Preferentially enhancing anti-cancer isothiocyanates over glucosinolates in broccoli sprouts: How nacl and salicylic acid affect their formation. Plant Physiol Biochem. 2017;115:343–53.
24. Kokotou MG, Revelou P-K, Pappas C, Constantinou-Kokotou V. High resolution mass spectrometry studies of sulforaphane and indole-3-carbinol in broccoli. Food Chem. 2017;237:566–73.
25. Ares AM, Ayuso I, Bernal JL, Nozal MJ, Bernal J. Trace analysis of sulforaphane in bee pollen and royal jelly by liquid chromatography–tandem mass spectrometry. J Chromatogr B. 2016;1012:130–6.
26. Chen S-Y, Wei W, Yin B-C, Tong Y, Lu J, Ye B-C. Development of a highly sensitive whole-cell biosensor for arsenite detection through engineered promoter modifications. ACS Synthetic Biology. 2019;8:2295–302.
27. Dhyani R, Shankar K, Bhatt A, Jain S, Hussain A, Navani NK. Homogentisic acid-based whole-cell biosensor for detection of alkaptonuria disease. Anal Chem. 2021;93:4521–7.
28. Yao J, He Y, Su N, Bharath SR, Tao Y, Jin J-M, et al. Developing a highly efficient hydroxytyrosol whole-cell catalyst by de-bottlenecking rate-limiting steps. Nat Commun. 2020;11:1–12.
29. Poulou M, Bell D, Bozonelos K, Alexiou M, Gavalas A, Lovell-Badge R, et al. Development of a chromosomally integrated metabolite-inducible Leu3p-α-IPM "off-on" gene switch. PLoS One. 2010;5:e12488.
30. Fang X, Liu Q, Bohrer C, Hensel Z, Han W, Wang J, et al. Cell fate potentials and switching kinetics uncovered in a classic bistable genetic switch. Nat Commun. 2018;9:1–9.
31. Gardner TS, Cantor CR, Collins JJ. Construction of a genetic toggle switch in escherichia coli. Nature. 2000;403:339–42.
32. Li T, Dong Y, Zhang X, Ji X, Luo C, Lou C, et al. Engineering of a genetic circuit with regulatable multistability. Integr Biol. 2018;10:474–82.
33. Shui S, Gainza P, Scheller L, Yang C, Kurumida Y, Rosset S, et al. A rational blueprint for the design of chemically-controlled protein switches. Nat Commun. 2021;12:1–12.
34. Bothfeld W, Kapov G, Tyo KEJ. A glucose-sensing toggle switch for autonomous, high productivity genetic control. ACS Synthetic Biology. 2017;6:1296–304.
35. Dinh CV, Prather KLJ. Development of an autonomous and bifunctional quorum-sensing circuit for metabolic flux control in engineered escherichia coli. Proc Natl Acad Sci. 2019;116:25562–8.
36. Barbier I, Perez-Carrasco R, Schaerli Y. Controlling spatiotemporal pattern formation in a concentration gradient with a synthetic toggle switch. Mol Syst Biol. 2020;16:e9361.
37. Harbaugh SV, Goodson MS, Dillon K, Zabarnick S, Kelley-Loughnane N. Riboswitch-based reversible dual color sensor. ACS Synthetic Biology. 2017;6:766–81.
38. Han P, Ma Y, Fu Z, Guo Z, Xie J, Wu Y, et al. A dna inversion system in eukaryotes established via laboratory evolution. ACS Synthetic Biology. 2021;10:2222–30.
39. Ham TS, Lee SK, Keasling JD, Arkin AP. Design and construction of a double inversion recombination switch for heritable sequential genetic memory. PLoS One. 2008;3:e2815.
40. Chiu T-Y, Jiang J-HR. Logic synthesis of recombinase-based genetic circuits. Sci Rep. 2017;7:1–13.
41. Jovanovic M, Waite C, James E, Synn N, Simpson T, Kotta-Loizou I, et al. Functional characterization of key residues in

regulatory proteins HrpG and HrpV of pseudomonas syringae pv. tomato DC3000. Mol Plant-Microbe Interact. 2017;30: 656–65.

42. Kamal MM, Nazzal S. Development and validation of a HPLC-UV method for the simultaneous detection and quantification of paclitaxel and sulforaphane in lipid based self-microemulsifying formulation. J Chromatogr Sci. 2019;57:931–8.
43. Mangla B, Alam O, Rub RA, Iqbal M, Singh A, Patel KS, et al. Development and validation of a high throughput bioanalytical UPLC-MS/MS method for simultaneous determination of tamoxifen and sulphoraphane in rat plasma: Application to an oral pharmacokinetic study. J Chromatogr B. 2020;1152: 122260.
44. Matusheski NV, Wallig MA, Juvik JA, Klein BP, Kushad MM, Jeffery EH. Preparative HPLC method for the purification of sulforaphane and sulforaphane nitrile from brassica oleracea. J Agric Food Chem. 2001;49:1867–72.
45. Kushad MM, Brown AF, Kurilich AC, Juvik JA, Klein BP, Wallig MA, et al. Variation of glucosinolates in vegetable crops of brassica o leracea. J Agric Food Chem. 1999;47:1541–8.
46. Zhou X, Jiang B, Zhang Y, Shang J, Yang H. Development of an electrochemical biosensor for sulforaphane determination in carmine radish. Int. J. Electrochem. Sci. 2017;12:1797–807.

SUPPORTING INFORMATION

Additional supporting information can be found online in the Supporting Information section at the end of this article.

How to cite this article: Li R, Chen S, Li Y, Chen X, Ye B-C. Development of a "turn off–on" whole-cell biosensor for sulforaphane detection based on the ultrasensitive activator HrpRS. Biotechnol Appl Biochem. 2022;1–13. https://doi.org/10.1002/bab.2400